**Article:**
Sobrinos-Sanguino, M, Vélez, M, Richter, RP orcid.org/0000-0003-3071-2837 et al. (1 more author) (2019) Reversible Membrane Tethering by ZipA Determines FtsZ Polymerization in Two and Three Dimensions. Biochemistry, 58 (38). pp. 4003-4015. ISSN 0006-2960

https://doi.org/10.1021/acs.biochem.9b00378

# Reversible membrane-tethering by ZipA determines FtsZ polymerization in two and three dimensions

Marta Sobrinos-Sanguino,[1,3] Marisela Vélez[2], Ralf P. Richter[3,4,*], Germán Rivas[1,*]

*[1] Centro de Investigaciones Biológicas, Consejo Superior de Investigaciones Científicas (CSIC), Madrid, Spain; [2] Instituto de Catálisis y Petroleoquímica, CSIC, Madrid; [3] School of Biomedical Sciences, Faculty of Biological Sciences, School of Physics and Astronomy, Faculty of Mathematics and Physical Sciences, and Astbury Centre for Structural Molecular Biology, University of Leeds, United Kingdom; [4] Biosurfaces Lab, CIC biomaGUNE, San Sebastian, Spain*

* Corresponding authors: grivas@cib.csic.es (GR) and r.richter@leeds.ac.uk (RPR)

**Keywords:** bacterial cell division, model membrane, self-organization, spectroscopic ellipsometry, quartz crystal microbalance

ABSTRACT: In most bacteria, the early step of septum formation implies the association of soluble FtsZ polymers to the cytoplasmic membrane. ZipA, together with FtsA, provide membrane tethering to FtsZ in *Escherichia coli*, forming a dynamic proto-ring that serves as an assembly scaffold for the remaining elements of the divisome. Despite their importance for bacterial cell division, multivalent interactions between proto-ring elements at membrane surfaces remain poorly characterized in quantitative terms. Here we measured the binding of FtsZ to ZipA incorporated in supported lipid bilayers at controlled densities by using a combination of biophysical surface-sensitive techniques (quartz crystal microbalance and spectroscopic ellipsometry) and analyzed how ZipA density and FtsZ concentration control the state of assembly of FtsZ. We find that ZipA attachment enables FtsZ-GMPCPP (where GMPCPP is a GTP analogue with reduced hydrolysis) to assemble in

several distinct ways, that is: (i) two-dimensional polymerization at the membrane, and (ii) three-dimensional polymerization from the membrane into the solution phase where this may be associated with the formation of higher-order complexes. In these processes, ZipA is required to enrich FtsZ at the surface but the FtsZ bulk concentration defines which morphology is being formed. Moreover, we report a strong effect of the nucleotide (GDP vs GMPCPP/GTP) on the kinetics of ZipA-association/dissociation of FtsZ. These results provide insights on the mode of interaction of proto-ring elements in minimal membrane systems and contribute to complete our understanding of the initial events of bacterial division.

## INTRODUCTION

The FtsZ protein (FtsZ, UniprotKB P0A9A6), a self-assembling GTPase present in the cytoplasm of most bacteria, is a tubulin homologue and a central component of the *Escherichia coli* divisome, the molecular machinery driving cytokinesis [1, 2]. FtsZ interacts with additional proteins to form a dynamic ring at the cytoplasmic membrane, which acts as a scaffold to recruit the remaining elements of the divisome. *In vitro* studies have shown that GTP drives the ($Mg^{2+}$-dependent) concerted assembly of FtsZ monomers to form flexible single-stranded filaments with a narrow size distribution; they tend to further associate into higher order polymers whose final structural organization depends upon experimental conditions [3]. Like other cytoskeletal filaments, these polymers are dynamic with a GTP-dependent turnover of FtsZ, which is considered to be central for positioning and function of the mature division ring [1, 4].

For membrane attachment, FtsZ requires two additional proteins, FtsA and ZipA. Together they form the so-called proto-ring, the initial molecular assembly of the divisome [5, 6]. FtsA is an amphitropic protein that associates with the membrane by an ATP-driven process involving a short amphipathic peptide helix [7]. ZipA (ZipA, UniprotKB P77173) consists of a short N-terminal extracellular region, a transmembrane region, and an intracellular C-terminal FtsZ-interacting domain that is connected to the transmembrane region by a flexible linker region [8, 9]. The C-terminal end of FtsZ binds the tethering elements of the proto-ring (FtsA and ZipA) and also other FtsZ-regulating proteins such as MinC which inhibits FtsZ polymerization and hence FtsZ ring formation at undesired locations. Thus, the C-terminal region of FtsZ acts as a central hub integrating signals that modulate divisome assembly in *E. coli* [10].

Minimal membrane systems, such as nanodiscs, liposomes and supported lipid bilayers (SLBs), have been used as scaffolds to reconstitute different combinations of proto-ring subsets in order to test their functional properties [11]. Among them, SLBs have allowed studying the structural organization and dynamics of proto-ring elements at the membrane by surface sensitive techniques.

Firstly, FtsZ when tethered to an SLB through ZipA forms dynamic polymer networks that can reorganize by fragmentation, annealing and lateral condensation, as revealed by atomic force microscopy [12]. Secondly, the co-reconstitution of FtsZ and FtsA on SLBs resulted in the emergence of dynamic chiral vortices whose diameters resemble the bacterial circumference, as shown by total internal reflection fluorescence microscopy imaging [13]. These dynamics are compatible with treadmilling of the polar FtsZ fibers. Thirdly and more recently, it has been shown that this self-organization phenomenon is an intrinsic property of FtsZ alone when supplemented with a membrane anchor and the chemical energy afforded by nucleotide hydrolysis [14]. The surface density of FtsZ was found to be the key parameter controlling the assembly and destabilization of FtsZ polymers rendering the turnover of curved polymer bundles directional, which results in the emergence of the chiral dynamic patterns.

These density-dependent transitions, reminiscent of the large-scale collective patterns of self-propelled driven filaments, such as microtubules, highlight the impact of surface concentration of proto-ring membrane-tethered elements on modulating the behavior of FtsZ polymers. Along these lines, it has been shown that the shrinkage of ZipA-containing vesicles driven by dynamic FtsZ polymers only occurs above a certain threshold ZipA density [15], and that the binding of FtsZ to ZipA on lipid-coated microbeads is modulated by nucleotides and the ZipA concentration at the lipid membrane surface [16].

Despite the established importance of tethering to ZipA for FtsZ assembly, we lack a quantitative description of how ZipA surface density correlates with FtsZ binding and regulates FtsZ self-organization. Here we have used supported lipid bilayers to anchor a histidine (His)-tagged soluble variant of ZipA (sZipA) to address these questions. sZipA was found to have FtsZ binding properties comparable to the full-length protein when incorporated in lipid bilayer nanodiscs [17, 18], and can readily be incorporated into membrane model systems. Specifically, the density of anchoring sites was tuned by controlling the amount of tris-nitrilotriacetic acid (tris-NTA) functionalized lipids in the SLB to which sZipA binds specifically (**Fig. 1A**). Tris-NTA provides a more stable anchorage than

the conventional mono-NTA because of its higher affinity for His tags, especially convenient for immobilization of sZipA at very low densities [19].

This platform, in combination with quartz crystal microbalance (QCM-D) and spectroscopic ellipsometry (SE), is well suited to investigate how the interaction and assembly properties of FtsZ are influenced by the surface concentration of ZipA in the lipid membrane. These surface sensitive analytical tools have allowed us to measure the binding of FtsZ bearing GMPCPP (a slowly hydrolysable GTP analog) over a broad range of receptor surface densities and to determine the impact of FtsZ-ZipA complex formation on the assembly properties of GMPCPP-FtsZ polymers. These data enabled us to identify two distinct binding regimes associated with the growth of FtsZ polymers along the surface, or from the surface into the bulk solution, respectively. In addition, our study identifies a drastic yet hitherto unappreciated difference in the kinetics of association/dissociation events when FtsZ carries GTP and GDP, respectively.

## MATERIALS AND METHODS

**Buffer preparation**: All buffers were prepared in ultrapure water and degased before use in QCM-D and SE assays. Working buffer for vesicle preparation contained 10 mM HEPES at pH 7.4, and 150 mM NaCl. Working buffer for ZipA and FtsZ binding assays contained 50 mM Tris, 300 mM KCl and 5 mM $MgCl_2$ at pH 7.5. All buffer components were purchased from Sigma.

**Protein purification**: The proteins used in this work were grown and purified from *E. coli* cells (BL21 strain) as previously described (FtsZ in [20]; His-tagged ZipA in [17] and [18]). The soluble construct of ZipA with 6 His tags (sZipA) was produced by elimination of the hydrophobic N-terminal domain (first 25 amino acids) as described earlier [18]. Protein stocks were pooled and stored at -80 °C. The purity of sZipA and FtsZ was verified by SDS-PAGE ($MW_{FtsZ}$ = 40 kDa, $MW_{sZipA}$ = 36 kDa) (**Fig. S1 in the Supporting Material)**. Typically, FtsZ was obtained at high concentration (~500 μM) and sZipA was concentrated (~40 μM). Both proteins were dialyzed in buffer containing 50 mM Tris, 500 mM KCl and 5 mM $MgCl_2$ after purification. For the present studies, sZipA and FtsZ were diluted in buffer to final concentrations of 0.28 μM, and between 0.125 and 25 μM, respectively. Polymer formation was induced by the addition of 0.5 mM GMPCPP, purchased from Jena Bioscience (Jena, Germany).

**Liposome preparation**: Lyophilized dioleoylphosphatidylcholine (DOPC) was purchased from Avanti Polar Lipids (Alabaster, AL, USA). A lipid analog with two oleoyl tails and a chelator headgroup comprising three nitrilotriacetic acid moieties (tris-NTA) was prepared as described earlier [21] and kindly provided by Changjiang You and Jacob Piehler (Osnabrück University, Germany). Both lipids were dissolved in chloroform and mixed in the desired molar ratios (0, 0.1, 0.5, 1, 2 and 5% tris-NTA). Mixtures were dried, first under a stream of nitrogen gas and then in vacuum, and then resuspended in working buffer. Small unilamellar vesicles (SUVs) were prepared by sonication, as described previously [22]. SUVs at a stock concentration of 2 mg/ml were stored at 4 °C under argon and used for up to one month. Before use, vesicle suspensions were diluted to 50

μg/ml in working buffer supplemented with 2 mM $NiCl_2$. The $NiCl_2$ was used to load the NTA with $Ni^{2+}$ ions and also facilitated SLB formation.

**Quartz crystal microbalance with dissipation monitoring (QCM-D)**: QCM-D measures changes in resonance frequency, Δ*f*, and dissipation, Δ*D*, of a sensor crystal upon interaction of soft matter with its surface. The QCM-D response is sensitive to the mass (including coupled water) and the mechanical properties of the surface-bound layer [23]. Silica-coated QCM-D sensors (QSX303; Biolin Scientific, Västra Frölunda, Sweden) were cleaned by immersion in 2% sodium dodecyl sulfate (SDS) for at least 30 min, abundant rinsing with ultrapure water and blow-drying in nitrogen gas. Prior to use, sensors were activated in a UV/ozone environment (Bioforce Nanoscience, Ames, IA, USA) for at least 30 min.

QCM-D measurements were performed with a Q-Sense E4 system equipped with Flow Modules (Biolin Scientific) with flow rates of typically 10 μl/min controlled by a syringe pump (KD Scientific, Holliston, MA, USA), at a working temperature of 23 °C. Although Δ*f* and Δ*D* were collected at six overtones (*i* = 3, 5, 7, 9, 11, 13), only the changes in dissipation, Δ*D*, and normalized frequencies, $\Delta f = \Delta f_i/i$, for *i* = 5 are presented for clarity in the main figures. All other overtones provided qualitatively similar information.

**Film thickness determination from QCM-D data.** For dense monolayers of globular proteins such as sZipA, the film thickness can be estimated using the Sauerbrey relation, i.e. from $d = -C / \rho \times \Delta f$, where the density ρ = 1.2 g/cm$^3$ represents the protein film density to within an error of less than 20% and $C$ = 18 ng/cm$^2$/Hz is the sensor's mass sensitivity constant [23]. For soft films of interpenetrating polymers such as 3D polymerized FtsZ (*vide infra*), data analysis with a continuum viscoealastic model is appropriate: thickness *d* and viscoelastic properties of the sZipA/FtsZ film were determined by fitting of the QCM-D data (comprising Δ*f* and Δ*D* for the 6 measured overtones) to a continuum viscoelastic model [24] as implemented in the software QTM [25] ('small load approximation'; D. Johannsmann, Technical University of Clausthal, Clausthal-Zellerfeld, Germany).

Viscoelastic properties were parameterized in terms of the shear storage modulus $G'(f)$ and the shear loss modulus $G''(f)$. The frequency dependencies of the storage and loss moduli were assumed to follow power laws within the measured range of 15 to 65 MHz, with exponents α' and α'', such that $G(f) = G_0 (f/f_0)^{\alpha}$, respectively, with $f_0$ set to 15 MHz. The exponents were confined to the ranges $0 \leq \alpha' \leq 2$ and $-1 \leq \alpha'' \leq 1$, i.e. the ranges physically reasonable for polymer solutions and gels [26]. The film density was assumed to be 1.0 g/cm$^3$. The fitting procedure was described in detail previously [27]; care was taken to analyse the confidence intervals for each of the fitted parameters, and the indicated errors correspond to a confidence level of one standard deviation. The thickness values obtained with the Sauerbrey relation and the viscoelastic model are expected to be comparable to the hydrodynamic film thickness [23]. For partial monolayers of discrete particles, such as sub-monolayers of sZipA (and likely also FtsZ 2D polymers; *vide infra*), neither of the above described analysis approaches is appropriate to accurately quantify film thickness [23]. Moreover, it is generally difficult to quantify the surface density of proteins by QCM-D because hydrodynamically coupled solvent also contributes to the QCM-D response and its relative contribution to the total measured mass is a priori unknown [23]. We thus used spectroscopic ellipsometry instead to quantify protein surface densities and estimate film thickness trends across the FtsZ 2D and 3D growth regimes.

**Spectroscopic ellipsometry (SE)**: SE measures changes in the polarization of light upon reflection from a surface. The SE response is sensitive to the thickness and refractive index of surface-bound layers. Silicon wafers were used as a support for SLBs and to attach proteins of interest. The wafers were cleaned by sequential rinsing with acetone, ethanol and ultrapure water; and subsequently activated with UV/ozone for 30 min.

SE measurements were carried out at room temperature in the same buffer as for the QCM-D experiments, with a M2000V system (J. A. Woollam, Lincoln, NE, USA; wavelength range λ = 380–1000 nm; horizontal plane of incidence; 70° angle of incidence) using a custom-built open cuvette (~120 µL volume; made from PEEK polymer with glass windows). The cuvette featured a magnetic

stirrer for continuous homogenization of the cuvette content and a flow-through tubing system for rapid solution exchange during rinsing steps [28, 29]. Prior to the measurement, the cuvette was passivated with 10 mg/mL bovine serum albumin (BSA; Sigma) diluted in water, rinsed with ultrapure water and blow-dried with nitrogen gas. Small volumes of concentrated samples were pipetted directly into the buffer-filled cuvette (without any flow through) and the magnetic stirrer then ensured rapid (i.e. within a few seconds) homogenization of the cuvette content and dilution of the sample to the desired concentration. Rinsing with buffer was performed with a peristaltic pump at a flow rate of 350 µl/min.

**Analysis of protein surface density and film thickness from SE data.** Data were analyzed with the software CompleteEASE (J. A. Woollam) using a model of multiple optically homogeneous layers, as described in detail elsewhere [22, 28]. Briefly, the protein film (made from sZipA alone, or from sZipA and FtsZ) was treated as a transparent Cauchy medium with an effective optical thickness $d_{eff}$ and a wavelength-dependent effective refractive index $n_{F,eff}(\lambda) = A_{F,eff} + B_F / \lambda^2$. The bulk solution was treated as a transparent Cauchy medium with $n_S(\lambda) = A_S + B_S / \lambda^2$. We set $A_S$ = 1.325 for the HEPES buffer with 150 mM NaCl (pure water contributes 1.322, and the salt 0.003), and 1.328 for TRIS buffer with 300 mM NaCl (pure water contributes 1.322, and the salt 0.006). We used $B_S = B_F$ = 0.00322 µm$^2$ where this is the dispersion of pure water and the contributions of salt and protein can be neglected [28]. $d_{eff}$ and $A_{F,eff}$ were the adjustable fit parameters.

Protein surface densities were determined through de Fejter's equation [30], $\Gamma = d_{eff}\, \Delta n_{eff} / (M_w \times dn/dc)$, where $M_w$ is the molecular mass, and $\Delta n_{eff}$ is the difference in refractive index between the protein film and the buffer solution ($\Delta n_{eff} = n_{F,eff}(\lambda) - n_S(\lambda) = A_{F,eff} - A_S$). We used a refractive index increment of $dn/dc$ = 0.180 cm$^3$/g for all proteins [31].

It shall here be noted that the film thickness obtained from SE with the above-described fitting should be considered an effective quantity and is therefore denoted as $d_{eff}$ throughout. Firstly, its determination is based on the assumption that the film is of constant protein concentration

throughout. We do not know what the morphology of the polymerized FtsZ is. It appears plausible that whilst the protein concentration is roughly constant for 2D polymerized FtsZ it would decrease gradually with the distance from the surface for 3D polymerized FtsZ. Under the latter conditions, the effectively measured optical thickness is expected to underestimate the geometric/hydrodynamic film thickness [32]. Secondly, the optical thickness of the protein film depends also on the optical properties of the substrate which are typically determined from SE data prior to protein incubation: considering possible errors on the substrate optical properties we estimate that the measured protein film thickness may be inaccurate by several nm (Ralf P. Richter, *personal communication*). We stress, however, that the resolution in the optical thickness is typically about 1 nm [31] and trends in film thickness can thus be measured reliably once the substrate optical properties are fixed. Moreover, whilst errors in the optical thickness may be appreciable these have only a marginal effect on the protein surface densities because any errors in $d_{eff}$ are compensated by errors in $A_{F,eff}$ such that the product $d_{eff}\ \Delta n = d_{eff}\ (A_{F.eff} - A_S)$ remains constant to a good approximation.

**Hill analysis**: Curves of sZipA/FtsZ effective film thickness $d_{\mathrm{eff}}$ vs. FtsZ concentration $c$ (thickness 'isotherms') were analyzed using a Hill equation with offset, that is, $d_{\mathrm{eff}} = d_{0,\mathrm{eff}} + d_{\mathrm{max,eff}}\frac{c^n}{K_{0.5}^n + c^n}$. Here, $K_{0.5}$ is the concentration at half-maximal binding, $n$ is the Hill coefficient, and $d_{0,\mathrm{eff}}$ and $d_{\mathrm{max,eff}}$ are the effective film thickness values in the limit of low and high FtsZ coverage, respectively. These four parameters were adjustable in the fitting.

Curves of the FtsZ surface density $\Gamma$ vs. FtsZ concentration $c$ (binding isotherms) were analyzed with a set of two Hill terms, that is $\Gamma = \Gamma_{2\mathrm{D}}\frac{c^{n_{2\mathrm{D}}}}{K_{2\mathrm{D}}^{n_{2\mathrm{D}}} + c^{n_{2\mathrm{D}}}} + \Gamma_{3\mathrm{D}}\frac{c^{n_{3\mathrm{D}}}}{K_{3\mathrm{D}}^{n_{3\mathrm{D}}} + c^{n_{3\mathrm{D}}}}$. Here, the index 2D represents the first phase of FtsZ binding (binding and polymerization at the surface) and index 3D the second phase (polymerization from the surface into the bulk solution). In the fitting, $K_{3\mathrm{D}}$ and $n_{3\mathrm{D}}$ were fixed

at the values obtained from the effective thickness isotherms, and $\Gamma_{2D}$, $K_{2D}$, $n_{2D}$ and $\Gamma_{3D}$ were adjustable in the fitting.

## RESULTS

### Preparation of model membranes

The proper assembly of model membranes displaying sZipA was confirmed by QCM-D (**Figs. 1B and S2**). SLBs were formed by the method of vesicle spreading (**Fig. 1B**, 4 to 20 min): a transient minimum in the frequency shift and a transient maximum in the dissipation shift reflect the binding of initially intact vesicles which subsequently rupture and coalesce into complete SLBs; the shifts of $\Delta f$ = -25 ± 2 Hz and $\Delta D \approx 0.2 \pm 0.1 \times 10^{-6}$ at the end of the vesicle incubation process are consistent with the formation of SLBs of good quality [33]. Injection of sZipA (**Fig. 1B**, 40 to 100 min) on SLBs prepared with vesicles containing 5 mol-% tris-NTA lipids generated an additional frequency shift of $\Delta f \approx$ -63 Hz. This corresponds to a hydrodynamic layer thickness of ~9 nm, consistent with the dimensions of the sZipA construct (a globular domain of ~3 nm diameter concatenated to a flexible region that can be folded, according to [9]). The relatively high associated dissipation shift ($\Delta D \approx 5 \times 10^{-6}$) can be ascribed to the presence of the flexible linker that connects the globular FtsZ binding domain to the SLB [34, 35] and provides compliance to the protein film. Only a minor fraction of sZipA was released upon rinsing with buffer (**Fig. 1B**, 100 to 120 min), whilst the rest remained bound upon rinsing with buffer but was readily eluted with imidazole (**Fig. S2**), indicating stable and specific anchorage through the His tags as desired.

The ZipA grafting density ($\Gamma_{ZipA}$) was quantified by spectroscopic ellipsometry (SE; **Fig. 1C**), and was found to be linearly dependent on the fraction of tris-NTA lipids in the vesicles from which the SLBs were prepared (**Fig. 1D**). $\Gamma_{ZipA}$ was here defined as the quasi-stable binding of sZipA after rinsing with buffer for at least 30 minutes. From these data, the mean spacing $s_{ZipA}$ between sZipA receptors could also be calculated (**Fig. 1D**, inset), demonstrating that a broad range of coverages,

from dense ($s_{ZipA}$ ≈ 5 nm for 5% tris-NTA) to very sparse ($s_{ZipA}$ ≈ 90 nm for 0.1% tris-NTA) packing are readily obtained.

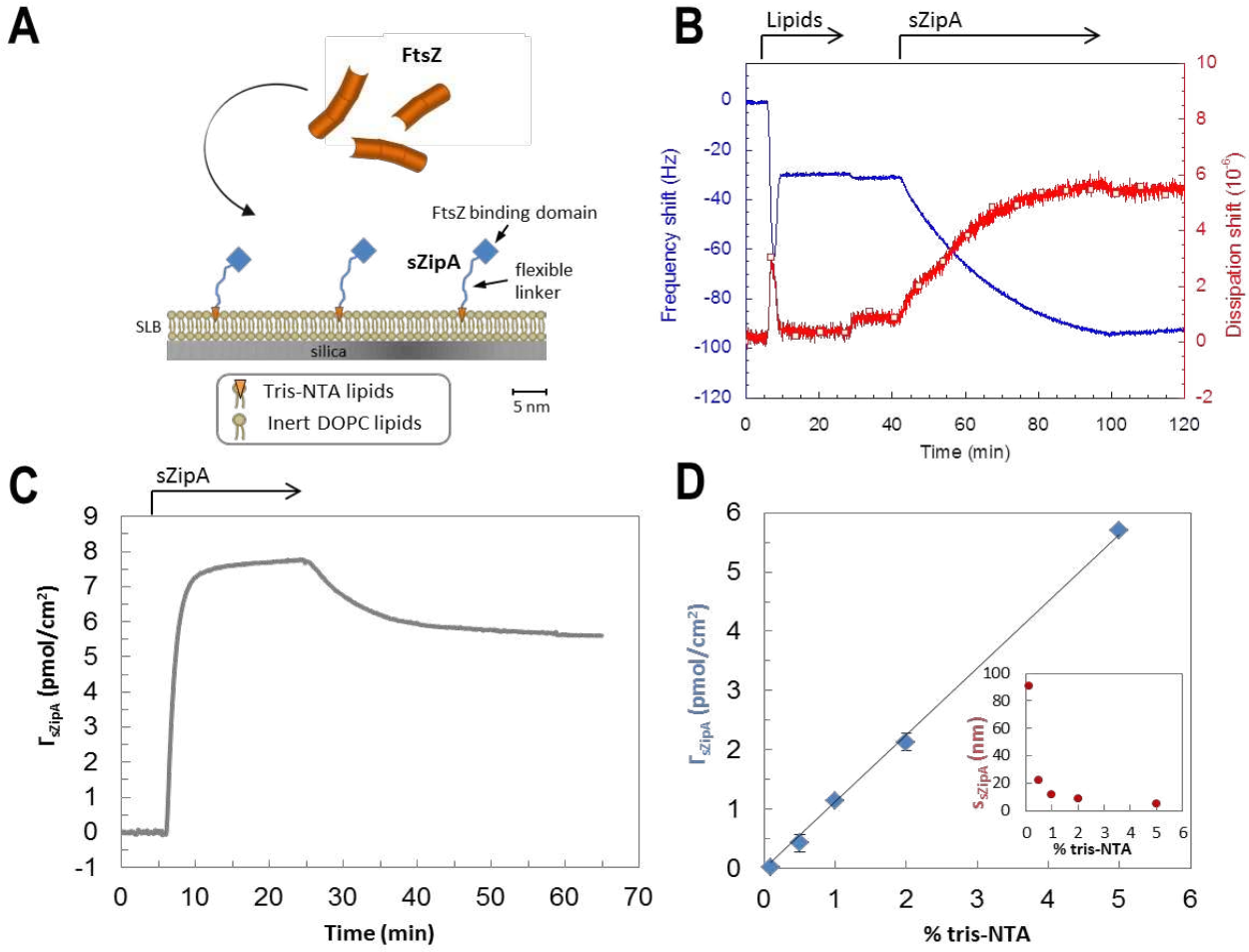


**FIG 1. Design of ZipA displaying model membranes. (A)** Scheme of bacterial sZipA-FtsZ interaction reconstituted on a silica-supported lipid bilayer (SLB). Protein and lipid sizes are drawn approximately to scale. **(B)** Preparation of a ZipA displaying SLB monitored by QCM-D (frequency shift - blue line, dissipation shift – red line with open symbols). **(C)** Time-resolved measurement of the ZipA grafting density ($\Gamma_{sZipA}$) by SE. Conditions for B and C: SUVs – 5% tris-NTA, 50 µg/ml; sZipA – 0.28 µM; start and duration of sample incubation steps are indicated with solid arrows on top of the plot; during remaining times the surfaces were exposed to plain working buffer. **(D)** sZipA grafting density post rinsing ($\Gamma_{sZipA}$, blue symbols) and corresponding average inter-sZipA spacing ($s_{sZipA}$, inset with red symbols; calculated as root-mean-square distance) as a function of tris-NTA content in the SLB (expressed in mol-% of tris-NTA lipids in the liposomes from which the SLBs were formed). Error bars represent standard deviations from at least two independent measurements. The black line is the result of a linear fit through the origin, giving a slope of 1.13 ± 0.02 pmol/cm² sZipA per % NTA.

## Quantification of FtsZ surface densities and identification of FtsZ polymer growth regimes on ZipA-displaying model membranes

To quantify FtsZ binding to sZipA-displaying model membranes, we performed titration assays by SE over a broad range of FtsZ concentrations (0.12 to 25 μM) and ZipA surface densities (0.5 to 5% tris-NTA, or 0.43 to 5.7 pmol/cm$^2$; cf. **Fig. 1D**). The formation of FtsZ polymers was elicited by the addition of GMPCPP (0.5 mM), a slowly hydrolysable GTP analogue [3]. FtsZ surface densities generally reached equilibrium within experimental time scales, as illustrated in **Fig. 2** for a selected sZipA surface density (5.7 pmol/cm$^2$). These assays revealed binding in a FtsZ-concentration and sZipA-surface-density dependent manner (**Fig. 3**). The equilibrium responses obtained by SE also facilitated analysis with equilibrium thermodynamic models. The binding isotherm of FtsZ-GMPCPP to 0.43 pmol/cm$^2$ sZipA, shown in **Fig. 3A**, revealed two discrete association processes occurring below and around the critical concentration for FtsZ polymerization in solution (1 μM), respectively. From the double-logarithmic presentation of the data, it can be appreciated that there are two separate phases in the isotherm with slopes well above 1 (below 0.25 μM, and between 0.75 and 1.5 μM FtsZ). This implies that FtsZ binding occurs in two distinct steps, each of which is positively cooperative. The distinctiveness of the two steps was most apparent at this low sZipA surface density yet it could also be discerned, with gradually decreasing sharpness, for the higher densities (**Fig. 3C**).

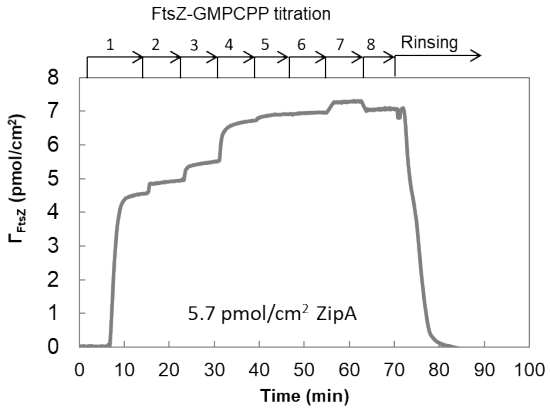


**FIG 2. Representative FtsZ-GMPCPP titration curve.** Surface density of FtsZ ($\Gamma_{FtsZ}$; quantified by SE) upon stepwise titration of a model membrane displaying 5.7 pmol/cm$^2$ sZipA with FtsZ. Model membrane preparation as in **Fig. 1B-C**; titration steps are labeled from 1 to 8, corresponding to FtsZ concentrations of 0.12, 0.25, 0.75, 1.5, 2.5, 5.0, 12.5 and 25 μM, respectively. Whilst FtsZ binding generally increased with FtsZ concentration, a minor decrease was observed upon switching from 12.5 to 25 μM FtsZ (step 7 to 8). It is not clear if this subtle reduction is real: for films thicker than a few 10 nm, SE becomes sensitive to the film density profile and changes in the density profile might entail an apparent change in surface density when analyzed with the simple optical model used here (which assumes a constant density across the film). Slightly negative surface densities post rinsing are likely due to release of some sZipA over the time course of the FtsZ titration and rinsing.

In addition to the protein surface density, SE also provides estimates of the protein film thickness. Interestingly, the measured effective thickness of the ZipA/FtsZ film also showed two distinct regimes (**Fig. 3B**): up to 0.5 μM FtsZ-GMPCPP the effective thickness was essentially constant (around 15 nm, i.e. roughly consistent with the size of a sZipA molecule in complex with a FtsZ molecule, taking into account the flexibility of the unstructured domain of ZipA), and above 0.5 μM FtsZ-GMPCPP it increased sharply to reach a new and much higher plateau value (around 40 nm, i.e. much larger than the size of such a simple complex). Similar thickness trends were found for all sZipA densities studied (**Fig. S3**). We ascribe the sharp increase in effective film thickness above 0.5 μM FtsZ-GMPCPP (**Fig. 3B**) to FtsZ polymerization with ZipA-bound FtsZ polymers emanating into the solution phase (3D polymerization) whilst the constant effective thickness up to 0.5 μM represented a two dimensional FtsZ film. We cannot however rule out that the higher density of filaments on the surface imposes a rearrangement of the nonstructured region of sZipA that could cause the extension of the flexible domain into the solution and thus make a (likely minor) contribution to the effective thickness increase [35]. The 3D thickness growth was found to be well described by a conventional Hill equation. The resulting association constant was $K_{0.5}$ = 1.18 ± 0.04 μM and the Hill coefficient was $n$ = 5.2 ± 0.4. These values should be considered effective for a couple of reasons. Firstly, the thickness values derived by SE are effective quantities: whilst they accurately reflect thickness trends, the absolute values should be interpreted with some caution: they may deviate from the hydrodynamic thickness of compact films (e.g. FtsZ in the 2D growth regime) by a few nanometers, and they may in addition substantially underestimate the hydrodynamic dimensions of graded films that exhibit a gradient of decreasing density from the surface into the solution (e.g. FtsZ in the 3D growth regime; see Methods for details). Secondly, it is not known if thickness is proportional to FtsZ surface density; however, both the $K_{0.5}$ value and the high degree of cooperativity are fully consistent with previous reports on FtsZ polymerization in solution (reviewed in [36]).

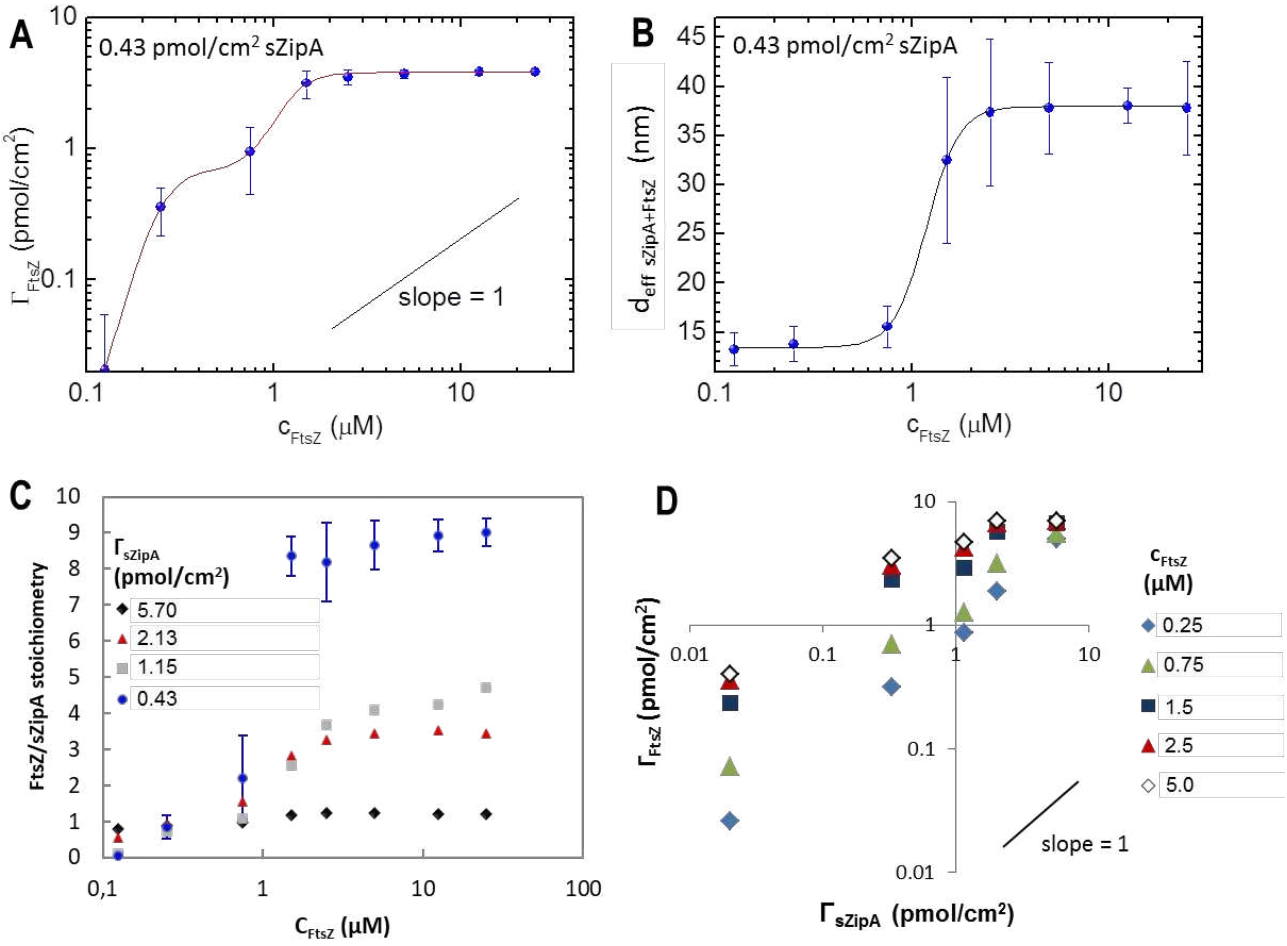


**FIG 3. Quantification of FtsZ-GMPCPP binding to ZipA-displaying model membranes by SE. (A-B)** Equilibrium binding data for an sZipA surface density of 0.43 pmol/cm² (0.5% tris-NTA), with mean and minima/maxima of at least two independent measurements: **(A)** Surface density of FtsZ ($\Gamma_{FtsZ}$) as a function of FtsZ concentration ($c_{FtsZ}$; in this double-logarithmic plot, a dashed line with a slope of 1 is shown for reference); **(B)** Effective sZipA/FtsZ film thickness, $d_{eff,sZipA+FtsZ}$, as a function of FtsZ concentration. Red lines are best fits to the data with Hill equations: the thickness data in **B** was fit with one Hill term plus offset and gave $K_{0.5} = 1.18 \pm 0.04$ μM and $n = 5.2 \pm 0.4$; the surface density data in **A** was fit with two Hill terms with $K_{3D}$ and $n_{3D}$ fixed at the values obtained from **B**, giving $\Gamma_{2D} = 0.68 \pm 0.20$ pmol/cm², $K_{2D} = 0.24 \pm 0.04$ μM, $n_{2D} = 5.2 \pm 1.1$ and $\Gamma_{3D} = 3.1 \pm 0.3$ pmol/cm². **(C)** FtsZ/sZipA binding stoichiometry as a function of FtsZ concentration for different sZipA surface densities (0.43 to 5.7 pmol/cm², as indicated). All data are from individual measurements, except at 0.43 pmol/cm² sZipA where the mean and minima/maxima of two independent measurements are presented. **(D)** Equilibrium surface density of FtsZ as a function of sZipA grafting density at several FtsZ concentrations (0.5 to 5 μM, as indicated; in this double-logarithmic plot, a line with a slope of 1 is shown for reference). All data are from individual measurements.

The binding data (**Fig. 3A**) was modelled with a sum of two Hill terms (see Methods), in which the first term (index 2D) is attributed to 2D polymerization and the second term (index 3D) to 3D polymerization. Although all the parameters could not be determined simultaneously with good confidence, when $K_{3D}$ and $n_{3D}$ were fixed to the values obtained from the thickness analysis, all other parameters could be well determined within narrow confidence intervals. The results of this modeling exercise revealed that (i) the maximal binding for phase 1 ($\Gamma_{2D}$ = 0.68 ± 0.20 pmol/cm$^2$) is of a magnitude comparable to the surface density of ZipA (0.43 pmol/cm$^2$) and (ii) the Hill coefficient for 2D polymerization ($n_{2D}$ = 5.2 ± 1.1) is comparable to the Hill coefficient for 3D polymerization estimated from effective thickness analysis. In this case, the best-fit value of the association constant was found to be $K_{2D}$ = 0.24 ± 0.04 μM.

***Density of the FtsZ polymer film.*** The FtsZ surface density saturated at approximately 4 pmol/cm$^2$ (**Fig 3A**). If all FtsZ monomers were hypothetically organized in a single layer, then this would be equivalent to a root-mean-square distance between monomers of ~ 5.4 nm. The FtsZ monomer is ~ 4 nm long and ~ 5 nm wide [37], and the total amount of bound FtsZ would hence just about fit into a monolayer on the surface, even at the highest ZipA surface density. However, since we observe that the thickness of the protein layer increases substantially when the FtsZ concentration in solution is above 1 μM (as shown by SE, **Fig. 3B**, and QCM-D, **Fig. 4**) we can conclude that the protein crowding at the membrane is at most moderate, without discarding the contribution to the obtained thickness values given by potential rearrangement of the unstructured domain of ZipA.

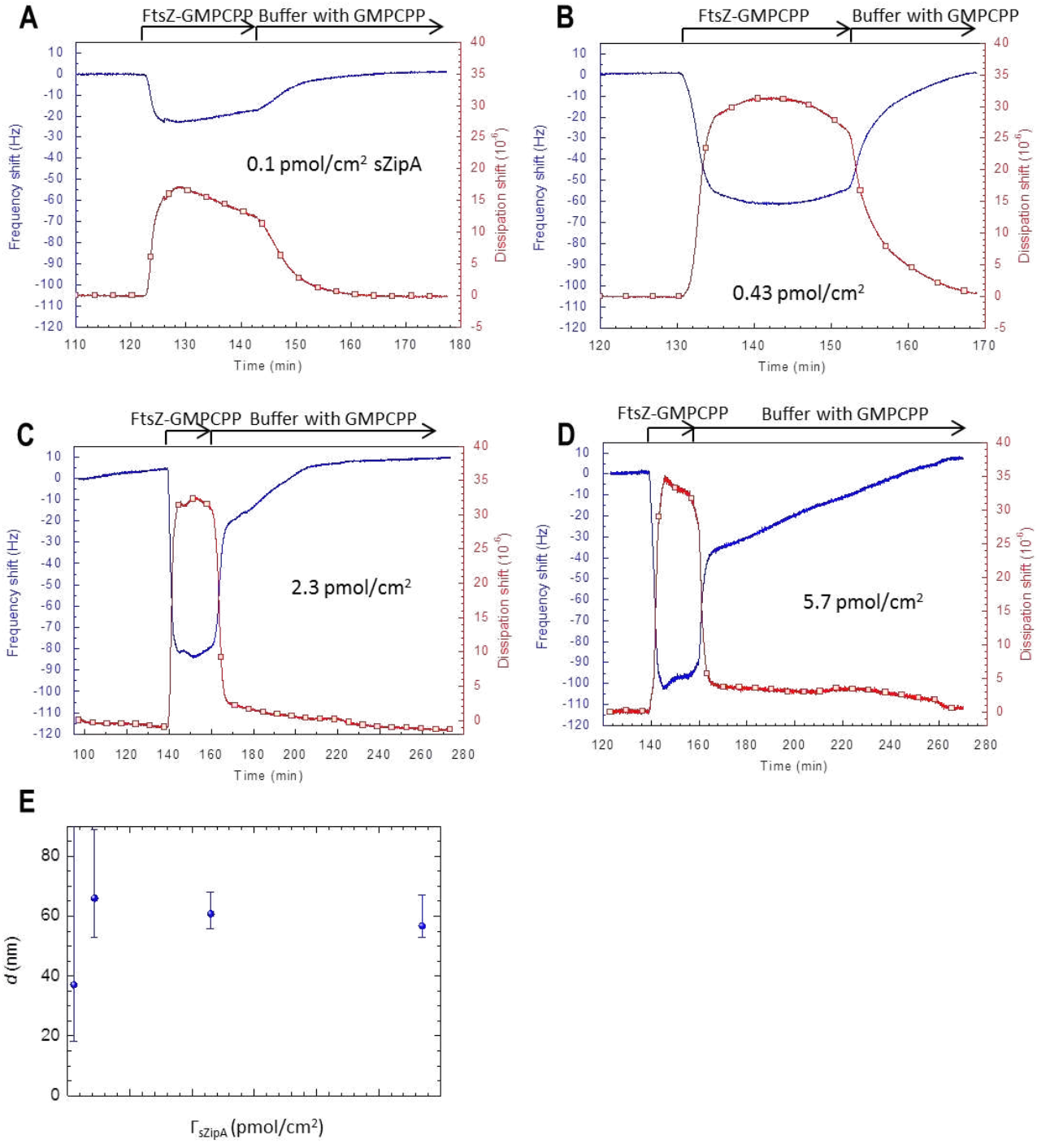


**FIG 4. QCM-D analysis of FtsZ-GMPCPP (polymer) binding as a function of ZipA surface density.** Shown are representative data (frequency shift - blue lines; dissipation shift - red lines with open symbols) for FtsZ binding and unbinding on four SLBs with distinct tris-NTA content (**A** - 0.1%, **B** - 0.5%, **C** - 2%, **D** - 5%) corresponding to a range of ZipA surface densities (0.1 to 5.7 pmol/cm$^2$, as indicated; see **Fig. 1D**). FtsZ was incubated at 10 μM with GMPCPP, and subsequent rinsing proceeded in GMPCPP-containing buffer (as indicated by arrows on top of the graphs). At all other times the surfaces were exposed to plain working buffer. See **Fig. S4** for complete data sets including SLB-formation, sZipA binding and washing steps. **(E)** sZipA/FtsZ film thickness, $d_{sZipA+FtsZ}$, as a function of sZipA surface density as obtained through viscoelastic modelling of QCM-D data. The time points during FtsZ incubation (in **A** to **D**) at which frequencies attained a minimum and dissipations a maximum were selected for fitting; see **Fig. S5** for the extracted film viscoelastic properties and the quality of the fit.

***Stoichiometry of ZipA-FtsZ binding.*** The SE data also enabled a direct quantitative comparison of the surface densities of FtsZ and sZipA, and hence allowed estimating the stoichiometry of binding of FtsZ-GMPCPP to sZipA. The results (**Fig. 3C**) reveal that binding was saturable for all tested sZipA surface densities. The maximal number of FtsZ subunits bound per sZipA was found to decrease substantially as the surface density of receptors increased, from a value close to 10 at 0.43 pmol/cm$^2$ sZipA (0.5% tris-NTA) to 1.0 at 5.7 pmol/cm$^2$ sZipA (5% tris-NTA). At 0.25 µM FtsZ, on the other hand, the stoichiometry varied only little, and remained below 1.0, across the full range of assayed sZipA surface densities. From these results, it can be concluded that almost all FtsZ molecules seem to be bound to ZipA in the first binding regime but in the second binding regime the majority of FtsZ oligomers is not directly bound to sZipA. Moreover, considering that a stoichiometry of 1.0 is attained for the highest sZipA density at saturation (i.e. where the film is too thick for all FtsZ molecules to contact sZipA), it appears that only a fraction of sZipA is occupied, meaning that binding in this case is limited by steric hindrance of the FtsZ polymers rather than by sZipA surface density.

***Sensitivity of FtsZ binding to ZipA surface density.*** To evaluate how sensitive FtsZ association is to ZipA coverage, we plotted $\Gamma_{FtsZ}$ against $\Gamma_{ZipA}$. The log-log plot (**Fig. 3D**) reveals that the slope of the curves does not increase significantly above 1 over the entire range of ZipA surface densities. This behavior contrasts what has previously been observed for thermodynamically stable and flexible polymers where the individually weak interactions of the polymer with multiple cell surface receptors entails a rather narrow dynamic range and a very sharp onset of binding at a certain receptor surface density (‘superselectivity’; [38]). The binding response of FtsZ varies gradually yet dynamically over the full range of possible ZipA receptor densities. Significant differences between this experimental setup and the one in which superselectivity was observed could explain this difference. A major difference is the reversible (i.e. continuously assembling and dissembling)

character of the FtsZ polymers. The interaction between FtsZ monomers triggered by the presence of GMPCPP is stronger than the interaction with ZipA [39] but also reversible. The slowly hydrolysable analogue slows down FtsZ monomer turnover [40] but does not eliminate it completely and this effect might still be present and affect locally the interaction with ZipA on the surface. Another possible explanation could be the lack of flexibility of the FtsZ polymers which may reduce the effective affinity of the individual FtsZ-ZipA interaction in a coverage-dependent manner owing to steric clashes between FtsZ polymers and to entropic penalties associated with the flexible ZipA membrane anchor needing to stretch to reach out and bind to a free FtsZ molecule. On the other hand, it is unlikely that the freedom of ZipA to diffuse across the membrane is responsible for the weak dependence of FtsZ binding on ZipA surface density, as receptor lateral mobility has previously been show to affect the quality of superselectivity only weakly [41].

**Morphology and reorganization of FtsZ polymer film**

***Specificity of binding.*** To complement the SE analysis and obtain further insight into the FtsZ polymerization process we also monitored FtsZ binding by QCM-D. These assays were performed as a single incubation step at 10 μM FtsZ-GMPCPP (**Fig. 4**). It is notable that a clear QCM-D response was observed even on 0.1% NTA (**Fig. 4A**) where the ZipA grafting density was at 0.1 pmol/cm$^2$ (i.e. close to the detection limit, with close to 100 nm average spacing between ZipA molecules; cf. **Fig. 1D**). In contrast, no binding of FtsZ was detected on SLBs lacking ZipA (**Fig. S2A**), indicating that FtsZ binds exclusively through sZipA to the model membranes. It has previously been shown that peptides derived from the C-terminal region of FtsZ containing the central hub region [42] inhibited the binding of FtsZ polymers to ZipA contained in nanodiscs [17]. Confirming the specificity of FtsZ binding, similarly, we found here that such peptides also compete with FtsZ polymers for binding to sZipA anchored to SLBs (**Fig. S2B**).

***Dynamic 3D polymerization and re-organization.*** A prominent feature observed for all ZipA surface densities was that FtsZ binding induced large dissipation shifts (**Fig. 4**). These provide further strong evidence for the 3D growth of FtsZ polymers, and thus corroborate the prior interpretation of the SE data (**Fig. 3B**). The dissipation shifts reached values of several $10 \times 10^{-6}$ which is much more than what is typically obtained for a simple monolayer of globular proteins: monolayers of streptavidin or green fluorescent protein tethered to a lipid bilayer, for example, produce dissipation shifts around $1 \times 10^{-6}$ [34, 43]. Shifts of several times $10^{-6}$ such as seen for sZipA monolayers (Fig. 1B) are already relatively high and usually due to extended flexible regions connecting the protein to the surface, or multiple protein domains to each other [34]. Dissipation shifts of $10 \times 10^{-6}$ and more, on the other hand, are readily attained with films of flexible polymers, such as one-end grafted 'brushes' of synthetic or biological polymers [32, 44, 45]. The very large dissipation shifts observed for FtsZ are thus incompatible with the formation of a simple protein monolayer and indicate that FtsZ instead binds to the surface forming a complex that emanates into the solution phase and generates a soft and relatively thick (and thus highly dissipative) polymer film.

Thickness values extracted by viscoelastic modelling of QCM-D data for films made of 10 μM FtsZ on several sZipA densities (**Figs. 4E** and **S5**) are of the same order of magnitude, yet moderately (about 50%) larger compared to the effective thickness values determined by SE (**Figs. 3B** and **S3**). This is consistent with FtsZ forming a graded layer with the density being highest near the surface and gradually decreasing into the solution phase, as for such films QCM-D is expected to provide a larger thickness than SE owing to the different contrast-sensing mechanisms of these two techniques [32]. This QCM-D thickness analysis suggests that the film thickness is virtually independent of sZipA surface density (**Fig. 4E**). The shear elastic modulus (elasticity), and to a lesser extend the loss modulus (proportional to viscosity), however, increase with ZipA (and consequently FtsZ) surface density (**Fig. S5A**) as would be expected for an increasingly dense film of interpenetrating polymers.

The QCM-D data upon FtsZ incubation at a single, high concentration (10 μM) also demonstrate that the polymer films assemble fast, as witnessed by the rapid decrease in frequency during the first few minutes after FtsZ injection. Another salient feature was that the QCM-D responses do not reach any equilibrium over the 20 min FtsZ incubation period. Instead, frequency and dissipation showed at least one transient extremum (in the case of 2% and 5% tris-NTA even several extrema) and following this the frequency slowly increased and the dissipation slowly decreased. This complex QCM-D response is in stark contrast to the SE data where we consistently observed binding equilibria being rapidly reached (**Fig. 2**). This can be understood by considering the different sensing principles of SE and QCM-D: whilst the areal mass density determined by SE is not (or at most weakly) influenced by the internal structure of the protein film, the QCM-D frequency shift is not only affected by the amount of FtsZ on the surface but also by the mechanical properties of the FtsZ film and the amount of hydrodynamically coupled solvent within it [23]. Joined together, the SE and QCM-D data thus indicate that the FtsZ polymer film reorganizes over extended incubation times although the FtsZ surface density remains approximately constant. Whilst QCM-D does not provide direct information about the ultrastructure of the polymer film, we can suggest based on the gross data that this reorganization reflects the formation of higher order polymer complexes such as the polymer bundles previously visualized by atomic force microscopy on SLBs [12].

It is notable that the complex QCM-D response was characteristic for high FtsZ concentrations (10 μM). When the FtsZ concentration was lowered to 0.5 μM, the magnitude of the QCM-D response was much smaller than at 10 μM but the binding readily attained equilibrium within 5 min of incubation (**Fig. 5A**). That the dissipation increased only marginally at 0.5 μM ($\Delta D \approx 1 \times 10^{-6}$, compared to $32 \times 10^{-6}$ at 10 μM) confirms that FtsZ polymers do no longer grow into the solution phase when the FtsZ concentration is lowered below the concentration required for polymerization in solution (1 μM at our working conditions [20]). Additional QCM-D experiments at 2.5 μM FtsZ (**Fig. 5A**) confirmed that there is a sharp, cooperative transition in the film morphology around 1 μM (**Fig. 5B**), consistent with the earlier SE data (**Fig. 3A-B**).

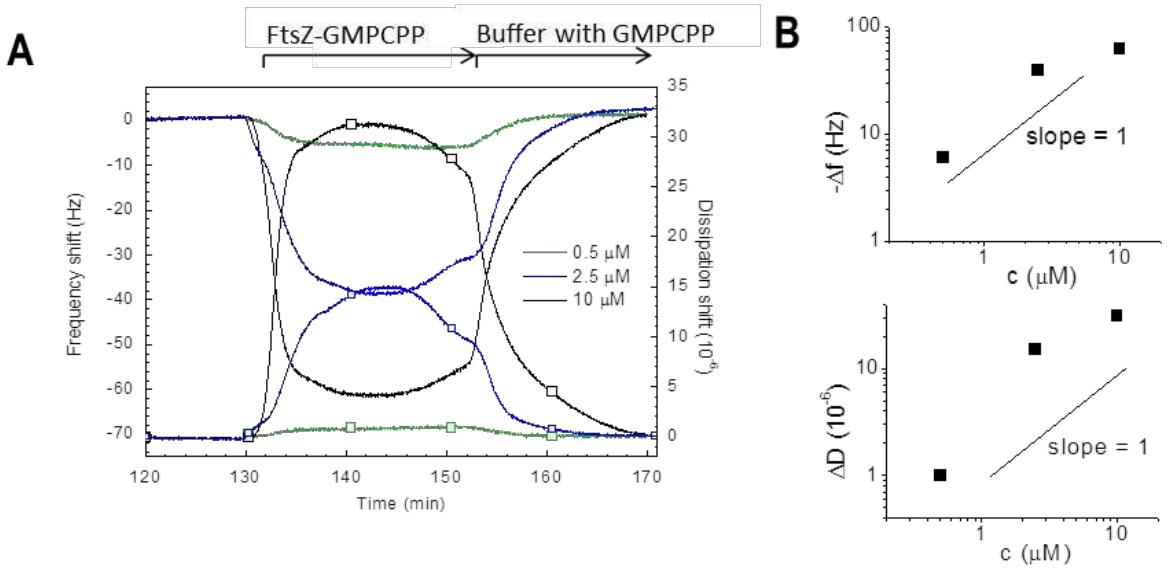


**FIG 5. Dependence of FtsZ-GMPCPP film morphology on FtsZ concentration. (A)** QCM-D data (frequency shift - solid lines, dissipation shift – solid lines with open squares) on model membranes with a selected sZipA grafting density (0.43 pmol/cm$^2$ sZipA, corresponding to 0.5 % tris-NTA) and three distinct FtsZ-GMPCPP concentrations (0.5 µM – green, 2.5 µM – blue, 10 µM – black). Start and duration of incubation with FtsZ are indicated with a solid arrow on top of the plot; during remaining times the surfaces were exposed to plain working buffer. **(B)** Minimal frequency shifts ($-\Delta f_{min}$) and maximal dissipation shifts ($\Delta D_{max}$) upon FtsZ binding as a function of FtsZ-GMPCPP concentration (from data in **A**); in these double-logarithmic plots, dashed lines with a slope of 1 are shown for reference: sharp changes with slopes larger than one between 0.5 and 2.5 µM are consistent with a cooperative transition within this concentration range.

***Dissociation.*** The dissociation of FtsZ-GMPCPP from the sZipA-displaying membrane, after rinsing with nucleotide-containing buffer, was fully reversible at all the receptor densities assayed (**Fig. 4**). Interestingly, whilst FtsZ dissociated in a single continuous event on SLBs with the lower sZipA densities (0.1% and 0.5% tris-NTA, corresponding to average distances between sZipA molecules of about 90 and 20 nm, respectively; **Fig. 4A-B**), the detachment occurred in two clearly distinct phases at the higher ZipA densities (2% and 5% tris-NTA, 10 and 5 nm; **Fig. 4C-D**). The frequency increased rapidly in the first phase (which lasted a few minutes) and much more slowly (and markedly linear) in the second phase. These two phases may correspond either to the release of two different polymer species or to polymer conformational changes during the dissociation process. Larger protein surface densities could favor more specific and stable lateral associations between filaments. That the dissipation shifts reached a level of only a few times $10^{-6}$ at the end of the first

phase (**Fig. 4C-D**) suggests that polymers that emanate into the solution phase dissociate in the first phase whilst polymers that are closely associated to the membrane are retained for longer and dissociate in the second phase.

**Interaction of FtsZ-GDP oligomers with sZipA-displaying model membranes**

Next, to assay the effect of the nucleotide bound to FtsZ on the kinetics of association to ZipA at the membrane and its subsequent dissociation from it, QCM-D experiments were performed in the presence of GDP instead of GMPCPP (**Fig. 6**). Under the conditions used in our assays (variable FtsZ concentrations in buffer with 300 mM KCl and 5 mM $MgCl_2$), FtsZ-GDP has been shown to self-associate and form short oligomers from monomers in a non-cooperative fashion, with hexamers being the largest species detectable [18].

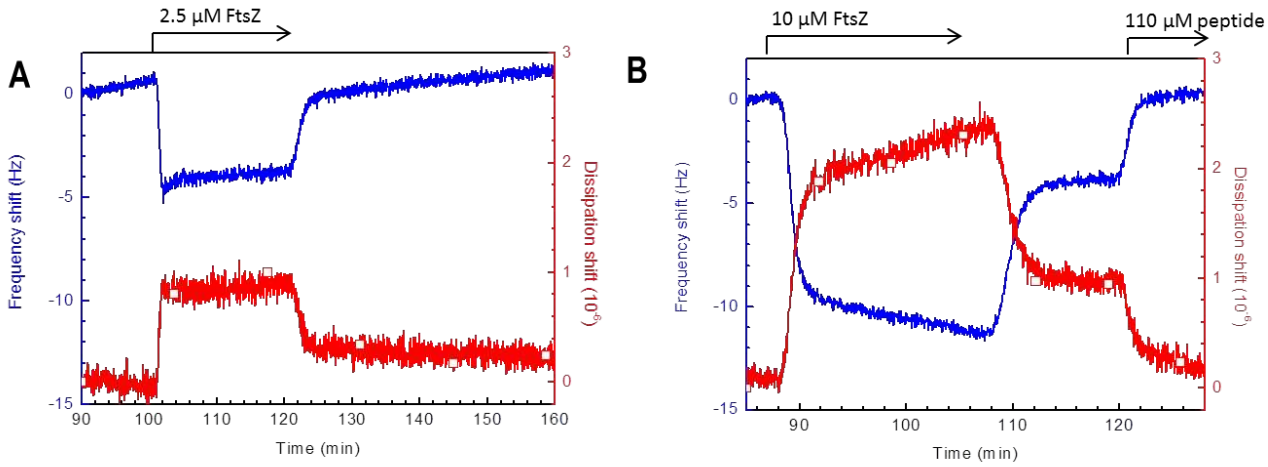


**FIG 6. FtsZ-GDP (oligomer) binding to ZipA-displaying model membranes.** QCM-D analysis (frequency shift – blue lines; dissipation shift – red lines with open symbols) of FtsZ-GDP binding to sZipA-displaying SLBs (0.5% tris-NTA, or 0.43 pmol/cm$^2$ sZipA): **(A)** 2.5 µM FtsZ-GDP, **(B)** 10 µM FtsZ-GDP and competition with FtsZ-derived peptide (110 µM). Arrows on top of the graphs indicate start and duration of injections with FtsZ-GDP or FtsZ-derived peptide, as indicated; during remaining times the surface was incubated with plain working buffer. Two-phase binding of FtsZ-GDP is evident in **B** but not **A**, and the FtsZ-derived peptide is able to fully displace the more stably bound fraction of FtsZ.

At 2.5 µM, FtsZ bound to sZipA-displaying model membranes (0.5% tris-NTA) in a single and rapid phase (**Fig. 6A**) which presumably corresponds to the binding of pre-formed FtsZ-GDP oligomers to sZipA. Such a phase was also observed at 10 µM with slightly larger magnitude, but a second

phase was additionally observed that was slow and did not saturate within the typical incubation time of 20 min in our experiments (**Fig. 6B**). This behaviour was unlike FtsZ-GMPCPP polymers, for which binding was fast and saturable (**Fig. 2**), and involved prolonged reorganization (**Fig. 4)**. The lack of saturation precluded a more detailed analysis of the binding process for FtsZ-GDP with thermodynamic models.

In contrast to FtsZ-GMPCPP polymers that were completely dissociated from ZipA during the washing step with buffer, at 0.5% sZipA and 10 μM FtsZ a significant fraction of FtsZ-GDP (corresponding to around 50% of the total bound protein) was found to remain stably bound. Interestingly, this fraction could be dislodged from the membrane by a molar excess of a C-terminal FtsZ peptide (**Fig. 6B**). This confirms that the bound FtsZ was specifically attached to sZipA via its genuine binding site. It highlights that the GDP-bound form of FtsZ dissociates more slowly from ZipA than the GTP/GMPCPP-bound form.

## DISCUSSION

Using supported lipid bilayers as minimal membrane systems, we here provided evidence that the binding of FtsZ-GMPCPP polymers to ZipA and the organization of the polymers at the membrane, are very sensitive to changes in FtsZ concentration yet rather insensitive to changes in ZipA concentration. We can argue that the primary parameter that bacteria use to control FtsZ ring formation is the local concentration of free FtsZ whereas modulation by ZipA surface density may aid in producing a robust response according to the moment of cell cycle.

How physiologically relevant are our minimal membrane systems? The SLBs reproduce the lateral mobility of bacterial membranes, allowing ZipA to diffuse freely and rearrange upon FtsZ binding. Moreover, our experiments were done in bilayers containing between 0.1 and 5% tris-NTA lipids to control the density of ZipA on the bilayer to be closer to physiological levels than in previous reconstitution experiments, in which 10% NTA was used [12, 13, 46]. In fact, the lowest surface density of ZipA used in our experiments (0.1 pmol/cm$^2$ on 0.1% tris-NTA) corresponds to ~400 molecules per μm$^2$. This closely matches what would be expected if the 1500 ZipA molecules that are typically present in *E. coli* covered the inner cell membrane area (~4 μm$^2$) uniformly. On the other hand, it has been estimated from *in vitro* assays that a local surface density of 10,000 ZipA molecules per μm$^2$ (equivalent to ~1.5% tris-NTA in our assay) is required for FtsZ induced membrane contraction [15].

On the basis of our results we propose a model of ZipA templated FtsZ-GPMCPP polymerization as shown in **Fig. 7** in which the assembly state depends rather sensitively on the concentration of FtsZ, and hence on its association state in solution. The concentration dependence of binding is best fit by two discrete yet similarly cooperative events. At concentrations below 0.1 μM, FtsZ would bind to surface-immobilized ZipA as monomers or linear oligomers. As the FtsZ concentration increases, these oligomers then grow in a single layer parallel to the surface, forming a two-dimensional assembly of polymers that cover the membrane. The increase in film thickness values detected by SE (**Fig. 3B**) and QCM-D (**Fig. 4E**), and in dissipation values detected by QCM-D (**Fig. 5B**), show

that, above 1 μM, the polymers also grow in the third dimension towards the bulk solution and likely form higher order structures such as bundles. A multilayered growth of FtsZ filaments on the surface at high protein concentration in solution has also been detected using fluorescence microscopy. Ramirez-Diaz et al. [47] described the formation of abundant three-dimensional polymer networks on the membrane when protein in solution was above 1.0 μM. Another useful surface characterization technique, Atomic Force Microscopy (AFM) could not, unfortunately, be used to confirm the presence of these protruding structures. Imaging soft, flexible filaments dynamically exchanging proteins present at high concentration in the imaging buffer is not technically feasible. However, images of a similar setup but in the absence of protein in the solution [12] already showed that the filament network was not lying completely flat on the lipid surface but that at some points filament bundles moved away from the surface. It is easy to imagine that in the presence of protein in solution, filament breaking observed could allow protein incorporation favoring further thickening and separation of the filaments from the surface.

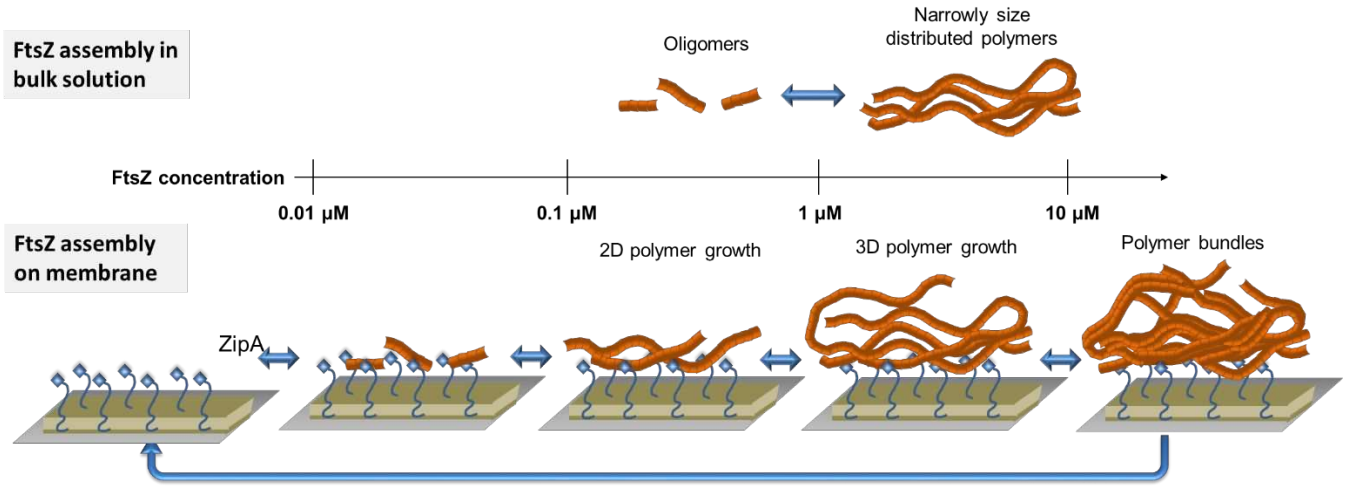


**FIG 7. Schematic illustration of the FtsZ polymerization and re-organization steps revealed in this study**. Scheme of the polymerization of FtsZ in bulk solution (upper panel) and on the surface (lower panel): In bulk solution, the FtsZ monomers and small oligomers assemble to form polymers above the critical concentration of polymerization in solution, around 1 μM. When attached to sZipA-displaying membranes, a two-phase polymerization occurs: below 1 μM, GMPCPP triggers FtsZ polymerization in 2 dimensions, assembling into polymers that grow parallel to the surface. Above 1 μM, the membrane-bound FtsZ preserves its ability to polymerize into the bulk solution, in 3 dimensions. The polymer film is thought to reorganize dynamically, and high local FtsZ concentrations may induce the formation of bundles due to lateral interactions between FtsZ polymers.

The equilibrium binding of FtsZ-GMPCPP polymers to ZipA-SLBs appears to be saturable at all ZipA surface densities assayed (Figs. 2-3). This observation agrees well with the previously reported behavior of the association of FtsZ-GTP polymers to ZipA contained in lipid-coated beads [16]. In both cases, binding saturability can be attributed to the composition of the polymers that the free FtsZ-GTP and FtsZ-GMPCPP form in solution, which show a narrow distribution of sizes (with weight-averaged stoichiometries around 100 and 200 for GTP and GMPCPP polymers, respectively [48]). We had previously proposed that the narrow size distribution could be a consequence of the formation of cyclic structures, that are not necessarily closed [36]. Consistent with such a scenario, the formation of chiral ring-like vortices of FtsZ on lipid membranes under conditions comparable to the ones used here has recently been described [47, 49]. It is interesting to note that this dynamic behavior was only observed when the protein concentration in solution was kept below 1 μM, corresponding to the regime in which the filaments are mostly lying parallel to the surface. At higher concentrations it is easy to visualize that the three dimensional growth could perturb the collective rotation of the vortexes parallel to the membrane plane.

Contrary to the GMPCPP form of FtsZ, the binding of FtsZ-GDP to ZipA did not equilibrate (Fig. 6). In a previous binding study using lipid-coated beads we had reported that FtsZ-GDP binding to ZipA-coated membranes does not to saturate, and proposed that this is due to surface associated FtsZ oligomers continuing to grow as the free FtsZ concentration increases [16]. This may also apply for the here-presented FtsZ-GDP binding data on planar membranes, and explain the continuous albeit slow second phase of binding.

We have also found that FtsZ-GMPCPP detaches from ZipA more easily than the FtsZ-GDP, despite the larger binding avidity of the FtsZ-GMPCPP polymers (and also FtsZ-GTP polymers [16]) to membrane-associated ZipA when compared to the binding of the FtsZ-GDP oligomers. In this way, a significant fraction of the GDP form remains stably attached to the surface and only can be dissociated by the addition of the FtsZ C-terminal peptide. Du et al. [50] have found that higher-order FtsZ-GDP oligomers bind more strongly to immobilized ZipA than the monomeric form. This

observed effect could explain the unexpected stability of the FtsZ-GDP oligomers remaining attached to the sZipA surface after rinsing.

These significant differences in the association/dissociation kinetics of both species may be due to the control by nucleotides of FtsZ association/assembly and its binding to ZipA (reviewed in [36]).

This differential behavior may have a biological implication for the bacterial cell cycle, related to the requirements of FtsZ at the vicinity of the membrane at the moment of proto-ring formation. Specifically, the GDP species presents a slowed-down binding rate in its second phase and also a slowed-down unbinding rate, while the GTP species (or the GMPCPP species in our assays) shows a more dynamic behavior, with quicker association/dissociation exchange rates. We may here hypothesize that the nucleotide effectively acts as a 'switch' activating the dynamism required to modulate the multiple interactions in which the C-terminus of FtsZ is involved acting as a central hub to integrate the signals that modulate the assembly of the division machinery for proper cell division.

In summary, we have developed a minimal membrane model on which the ZipA surface density was quantitatively tuned. Our results demonstrate that, at the ZipA densities tested, the binding of FtsZ-GMPCPP (and by extension –GTP) polymers, unlike FtsZ-GDP oligomers, is reversible and depends primarily on the free FtsZ concentration in solution. Free polymers can adopt higher-order structures in two and three dimensions, likely relevant for the formation of the FtsZ ring. The ZipA surface density plays a secondary role and probably provides a robust anchorage to FtsZ oligomers and polymers. The presented approach can easily be extended to other divisome elements or mixtures of them, and thus provides a robust tool for the screening of interactions with FtsZ in a relevant and well-controlled environment. Future studies will aim, in particular, at understanding the role of the C-terminus of FtsZ as a central hub integrating signals that modulate divisome assembly, and at elucidating the biochemical parameters that govern these multiple interactions at the proto-ring.

## AUTHORS CONTRIBUTIONS

MS-S performed experiments, participated in data analysis and drafted the manuscript. MV participated in the drafting of the manuscript, RPR and GR conceived the study, designed the experiments, participated in data analysis and drafted the manuscript. All authors gave final approval for publication.

## ACKNOWLEDGMENTS

We thank Jacob Piehler and Changjiang You (University of Osnabrück, Germany) for providing tris-NTA-functionalized lipids. We also thank members of the GR lab for technical assistance in protein purification and helpful discussion, and Galina Dubacheva (Ecole Nationale Superieure, Cachan, France) for pilot experiments leading to this work.

## FUNDING

This work was supported by the European Research Council (Starting Grant 306435 'JELLY', to RPR) and the Spanish Government through grant BFU2016-75471-C2-1-P (to GR).

## SUPPORTING INFORMATION

Supplementary figures (Fig. S1-S5)

## REFERENCES


1. Erickson, H.P., Anderson, D.E. and Osawa, M. (2010) FtsZ in bacterial cytokinesis: cytoskeleton and force generator all in one. *Microbiol Mol Biol Rev.* ***74****(4)*: p. 504-528.
2. Haeusser, D.P. and Margolin, W. (2016) Splitsville: structural and functional insights into the dynamic bacterial Z ring. *Nat Rev Microbiol.* ***14****(5)*: p. 305-319.
3. Ahijado-Guzman, R., Alfonso, C., Reija, B., Salvarelli, E., Mingorance, J., Zorrilla, S., Monterroso, B. and Rivas, G. (2013) Control by potassium of the size distribution of Escherichia coli FtsZ polymers is independent of GTPase activity. *J Biol Chem.* ***288****(38)*: p. 27358-27365.
4. Mingorance, J., Rivas, G., Velez, M., Gomez-Puertas, P. and Vicente, M. (2010) Strong FtsZ is with the force: mechanisms to constrict bacteria. *Trends Microbiol.* ***18****(8)*: p. 348-356.
5. Adams, D.W. and Errington, J. (2009) Bacterial cell division: assembly, maintenance and disassembly of the Z ring. *Nat Rev Microbiol.* ***7****(9)*: p. 642-653.
6. Rico, A.I., Krupka, M. and Vicente, M. (2013) In the beginning, Escherichia coli assembled the proto-ring: an initial phase of division. *J Biol Chem.* ***288****(29)*: p. 20830-20836.
7. Pichoff, S. and Lutkenhaus, J. (2005) Tethering the Z ring to the membrane through a conserved membrane targeting sequence in FtsA. *Mol Microbiol.* ***55****(6)*: p. 1722-1734.
8. Hale, C.A. and de Boer, P.A. (1997) Direct binding of FtsZ to ZipA, an essential component of the septal ring structure that mediates cell division in E. coli. *Cell.* ***88****(2)*: p. 175-185.
9. Ohashi, T., Hale, C.A., de Boer, P.A. and Erickson, H.P. (2002) Structural evidence that the P/Q domain of ZipA is an unstructured, flexible tether between the membrane and the C-terminal FtsZ-binding domain. *J Bacteriol.* ***184****(15)*: p. 4313-4315.
10. Pazos, M., Natale, P., Margolin, W. and Vicente, M. (2013) Interactions among the early Escherichia coli divisome proteins revealed by bimolecular fluorescence complementation. *Environ Microbiol.* ***15****(12)*: p. 3282-3291.
11. Schwille, P. (2014) Bacterial cell division: a swirling ring to rule them all? *Curr Biol.* ***24****(4)*: p. R157-159.
12. Mateos-Gil, P., Marquez, I., Lopez-Navajas, P., Jimenez, M., Vicente, M., Mingorance, J., Rivas, G. and Velez, M. (2012) FtsZ polymers bound to lipid bilayers through ZipA form dynamic two dimensional networks. *Biochim Biophys Acta.* ***1818****(3)*: p. 806-813.
13. Loose, M. and Mitchison, T.J. (2014) The bacterial cell division proteins FtsA and FtsZ self-organize into dynamic cytoskeletal patterns. *Nat Cell Biol.* ***16****(1)*: p. 38-46.
14. Ramírez, D., García-Soriano, D.A., Raso, A., Feingold, M., Rivas, G. and Schwille, P. (2016) Chiral vortex dynamics on membranes is an intrinsic property of FtsZ, driven by GTP hydrolysis. *bioRxiv.*
15. Cabre, E.J., Sanchez-Gorostiaga, A., Carrara, P., Ropero, N., Casanova, M., Palacios, P., Stano, P., Jimenez, M., Rivas, G. and Vicente, M. (2013) Bacterial division proteins FtsZ and ZipA induce vesicle shrinkage and cell membrane invagination. *J Biol Chem.* ***288****(37)*: p. 26625-26634.
16. Sobrinos-Sanguino, M., Zorrilla, S., Monterroso, B., Minton, A.P. and Rivas, G. (2017) Nucleotide and receptor density modulate binding of bacterial division FtsZ protein to ZipA containing lipid-coated microbeads. *Sci Rep.* ***7****(1)*: p. 13707.
17. Hernandez-Rocamora, V.M., Reija, B., Garcia, C., Natale, P., Alfonso, C., Minton, A.P., Zorrilla, S., Rivas, G. and Vicente, M. (2012) Dynamic interaction of the Escherichia coli cell division ZipA and FtsZ proteins evidenced in nanodiscs. *J Biol Chem.* ***287****(36)*: p. 30097-30104.
18. Martos, A., Alfonso, C., Lopez-Navajas, P., Ahijado-Guzmn, R., Mingorance, J., Minton, A.P. and Rivas, G. (2010) Characterization of self-association and heteroassociation of bacterial cell division proteins FtsZ and ZipA in solution by composition gradient-static light scattering. *Biochemistry.* ***49****(51)*: p. 10780-10787.

19. Lata, S., Reichel, A., Brock, R., Tampe, R. and Piehler, J. (2005) High-affinity adaptors for switchable recognition of histidine-tagged proteins. *J Am Chem Soc.* ***127****(29)*: p. 10205-10215.
20. Rivas, G., Lopez, A., Mingorance, J., Ferrandiz, M.J., Zorrilla, S., Minton, A.P., Vicente, M. and Andreu, J.M. (2000) Magnesium-induced linear self-association of the FtsZ bacterial cell division protein monomer. The primary steps for FtsZ assembly. *J Biol Chem.* ***275****(16)*: p. 11740-11749.
21. Beutel, O., Nikolaus, J., Birkholz, O., You, C., Schmidt, T., Herrmann, A. and Piehler, J. (2014) High-fidelity protein targeting into membrane lipid microdomains in living cells. *Angew Chem Int Ed Engl.* ***53****(5)*: p. 1311-1315.
22. Eisele, N.B., Frey, S., Piehler, J., Gorlich, D. and Richter, R.P. (2010) Ultrathin nucleoporin phenylalanine-glycine repeat films and their interaction with nuclear transport receptors. *EMBO Rep.* ***11****(5)*: p. 366-372.
23. Reviakine, I., Johannsmann, D. and Richter, R.P. (2011) Hearing what you cannot see and visualizing what you hear: interpreting quartz crystal microbalance data from solvated interfaces. *Anal Chem.* ***83****(23)*: p. 8838-8848.
24. Johannsmann, D. (1999) Viscoelastic analysis of organic thin films on quartz resonators. *Macromol. Chem. Phys.* ***200***: p. 501-516.
25. Johannsmann, D. *The software QTM is freely available for download (http://www2.pc.tu-clausthal.de/dj/software_en.shtml), with a tutorial and guide, and contains the algorithms described in http://www.pc.tuclausthal.de/en/research/johannsmann-group/qcm-modelling/*.
26. Rubinstein, M. and Colby, R.H., *Polymer Physis*. 2003: Oxford University Press: Oxford.
27. Eisele, N.B., Andersson, F.I., Frey, S. and Richter, R.P. (2012) Viscoelasticity of thin biomolecular films: a case study on nucleoporin phenylalanine-glycine repeats grafted to a histidine-tag capturing QCM-D sensor. *Biomacromolecules.* ***13****(8)*: p. 2322-2332.
28. Carton, I., Brisson, A.R. and Richter, R.P. (2010) Label-free detection of clustering of membrane-bound proteins. *Anal Chem.* ***82****(22)*: p. 9275-9281.
29. Migliorini, E., Thakar, D., Sadir, R., Pleiner, T., Baleux, F., Lortat-Jacob, H., Coche-Guerente, L. and Richter, R.P. (2014) Well-defined biomimetic surfaces to characterize glycosaminoglycan-mediated interactions on the molecular, supramolecular and cellular levels. *Biomaterials.* ***35****(32)*: p. 8903-8915.
30. De Feijter, J.A., Benjamins, J. and Veer, F.A. (1978) Ellipsometry as a tool to study the adsorption behavior of synthetic and biopolymers at the air-water interface. *Biopolymers.* ***17***: p. 1759-1772.
31. Richter, R., Rodenhausen, K.B., Eisele, N.B. and Schubert, M., *Coupling Spectroscopic Ellipsometry and Quartz Crystal Microbalance to Study Organic Films at the Solid-Liquid Interface*, in *Ellipsometry of Functional Organic Surfaces and Films*. 2018, Springer International Publishing AG: Berlin (Germany). p. 391-417.
32. Domack, A., Prucker, O., Ruhe, J. and Johannsmann, D. (1997) Swelling of a polymer brush probed with a quartz crystal resonator. *Phys Rev.* ***56***: p. 680-689.
33. Richter, R.P., Berat, R. and Brisson, A.R. (2006) Formation of solid-supported lipid bilayers: an integrated view. *Langmuir.* ***22****(8)*: p. 3497-3505.
34. Johannsmann, D., Reviakine, I. and Richter, R.P. (2009) Dissipation in films of adsorbed nanospheres studied by quartz crystal microbalance (QCM). *Anal Chem.* ***81****(19)*: p. 8167-8176.
35. Mateos-Gil, P., Tsortos, A., Velez, M. and Gizeli, E. (2016) Monitoring structural changes in intrinsically disordered proteins using QCM-D: application to the bacterial cell division protein ZipA. *Chem Commun (Camb).* ***52****(39)*: p. 6541-6544.
36. Monterroso, B., Alfonso, C., Zorrilla, S. and Rivas, G. (2013) Combined analytical ultracentrifugation, light scattering and fluorescence spectroscopy studies on the functional associations of the bacterial division FtsZ protein. *Methods.* ***59****(3)*: p. 349-362.
37. Lowe, J. and Amos, L.A. (1998) Crystal structure of the bacterial cell-division protein FtsZ. *Nature.* ***391****(6663)*: p. 203-206.

38. Dubacheva, G.V., Curk, T., Auzely-Velty, R., Frenkel, D. and Richter, R.P. (2015) Designing multivalent probes for tunable superselective targeting. *Proc Natl Acad Sci U S A.* ***112****(18)*: p. 5579-5584.
39. Huecas, S. and Andreu, J.M. (2003) Energetics of the cooperative assembly of cell division protein FtsZ and the nucleotide hydrolysis switch. *J Biol Chem.* ***278****(46)*: p. 46146-46154.
40. Hyman, A.A., Salser, S., Drechsel, D.N., Unwin, N. and Mitchison, T.J. (1992) Role of GTP hydrolysis in microtubule dynamics: information from a slowly hydrolyzable analogue, GMPCPP. *Mol Biol Cell.* ***3****(10)*: p. 1155-1167.
41. Dubacheva, G.V., Curk, T., Frenkel, D. and Richter, R.P. (2019) Multivalent Recognition at Fluid Surfaces: The Interplay of Receptor Clustering and Superselectivity. *J Am Chem Soc.* ***141****(6)*: p. 2577-2588.
42. Ortiz, C., Natale, P., Cueto, L. and Vicente, M. (2016) The keepers of the ring: regulators of FtsZ assembly. *FEMS Microbiol Rev.* ***40****(1)*: p. 57-67.
43. Bingen, P., Wang, G., Steinmetz, N.F., Rodahl, M. and Richter, R.P. (2008) Solvation effects in the quartz crystal microbalance with dissipation monitoring response to biomolecular adsorption. A phenomenological approach. *Anal Chem.* ***80****(23)*: p. 8880-8890.
44. Richter, R.P., Hock, K.K., Burkhartsmeyer, J., Boehm, H., Bingen, P., Wang, G., Steinmetz, N.F., Evans, D.J. and Spatz, J.P. (2007) Membrane-grafted hyaluronan films: a well-defined model system of glycoconjugate cell coats. *J Am Chem Soc.* ***129****(17)*: p. 5306-5307.
45. Zahn, R., Osmanovic, D., Ehret, S., Araya Callis, C., Frey, S., Stewart, M., You, C., Gorlich, D., Hoogenboom, B.W. and Richter, R.P. (2016) A physical model describing the interaction of nuclear transport receptors with FG nucleoporin domain assemblies. *Elife.* ***5***: p. e14119.
46. Marquez, I.F., Mateos-Gil, P., Shin, J.Y., Lagos, R., Monasterio, O. and Velez, M. (2017) Mutations on FtsZ lateral helix H3 that disrupt cell viability hamper reorganization of polymers on lipid surfaces. *Biochim Biophys Acta Biomembr.* ***1859****(10)*: p. 1815-1827.
47. Ramirez-Diaz, D.A., Garcia-Soriano, D.A., Raso, A., Mucksch, J., Feingold, M., Rivas, G. and Schwille, P. (2018) Treadmilling analysis reveals new insights into dynamic FtsZ ring architecture. *PLoS Biol.* ***16****(5)*: p. e2004845.
48. Monterroso, B., Ahijado-Guzman, R., Reija, B., Alfonso, C., Zorrilla, S., Minton, A.P. and Rivas, G. (2012) Mg(2+)-linked self-assembly of FtsZ in the presence of GTP or a GTP analogue involves the concerted formation of a narrow size distribution of oligomeric species. *Biochemistry.* ***51****(22)*: p. 4541-4550.
49. Krupka, M., Sobrinos-Sanguino, M., Jimenez, M., Rivas, G. and Margolin, W. (2018) Escherichia coli ZipA Organizes FtsZ Polymers into Dynamic Ring-Like Protofilament Structures. *MBio.* ***9****(3)*: p. 01008-01018.
50. Du, S., Park, K.T. and Lutkenhaus, J. (2015) Oligomerization of FtsZ converts the FtsZ tail motif (conserved carboxy-terminal peptide) into a multivalent ligand with high avidity for partners ZipA and SlmA. *Mol Microbiol.* ***95****(2)*: p. 173-188.

**For Table of Contents Only**